Phase behavior of Ising mixtures

W. Fenz and R. Folk
Institute for Theoretical Physics, Linz University, A-4040 Linz, Austria
(Received 23 November 2004; published 4 April 2005)

We present phase diagrams that were calculated both in mean-field theory and via Monte Carlo (MC) simulations for binary mixtures of a ferromagnetic Ising fluid and a nonmagnetic fluid (Ising mixtures) in the absence of an external field. We look at both the simple ideal Ising mixture, consisting of an ideal Ising fluid and a hard-sphere fluid, as well as at the general case with one component being a nonideal Ising fluid and the other a van der Waals fluid. It is shown that the mean-field phase diagram of the ideal Ising mixture in the limit of infinite pressure is identical to that of the Blume-Capel model for ^{3}He-^{4}He mixtures. The MC phase diagrams were obtained using the Gibbs ensemble, the cumulant intersection technique, and the multihistogram reweighting method, adapted to the semigrand ensemble. The results are qualitatively compared with mean-field theory, and both types of tricritical lines occurring there are verified in the computer simulations.

DOI: 10.1103/PhysRevE.71.046104 PACS number(s): 64.60.Kw, 75.50.Mm, 61.20.Ja

I. INTRODUCTION

While there are, apart from undercooled droplets of certain exotic metal alloys [1,2], no realistic examples of ferromagnetic fluids known today, the study of phase transitions in magnetic fluids and their mixtures is still of great value and interest, due to several reasons. First of all, the magnetic fluid can serve as a simplified model for other real systems showing a similar phase behavior. Some examples would be dipolar fluids, which are often studied using the more realistic Stockmayer fluid model [3–5], or ionic fluids, commonly described by the so-called restricted primitive model (RPM) [6,7]. Both these systems exhibit phase diagram topologies that are also obtained within the magnetic fluid model.

Another system that can be described with magnetic fluids is the ^{3}He-^{4}He mixture. In this case, the spin degree of freedom corresponds to the superfluid order parameter of the ^{4}He component. Since the actual order parameter—the complex superfluid wave function—is two dimensional, the best model would be a mixture of an *XY* spin fluid and a nonmagnetic fluid. However, a simple Ising spin, as applied in the Blume-Emery-Griffiths (BEG) lattice model for ^{3}He-^{4}He mixtures [8], already provides the correct topology of the phase diagram. The so-called vectoralized BEG (VBEG) model [9–11], using *XY* spins instead, exhibits similar phase behavior. If one is interested in the universal quantities associated with critical phenomena, on the other hand, the choice of the spin dimensionality is of course essential. As will be shown in this paper, the mixture of an ideal Ising fluid and a nonmagnetic fluid in mean-field theory can be considered as a generalization of the BEG model to the continuum, yielding the BEG phase diagrams in the limit of infinite pressure (the phase behavior of mixtures at extremely high pressures is also of interest in chemical physics; see [12]).

Another interesting feature that is unique to the Ising fluid model is the fact that it can be mapped exactly onto a symmetrical (nonmagnetic) binary mixture [13,14]. Since there are only two possible states for the spin, +1 and −1, one can regard spin-up and spin-down particles as two different species, having identical interactions with particles of the same kind, but a different one with particles of the other component. The magnetization then corresponds to the concentration of the mixture, and the magnetic field to the chemical potential difference of the two species. Results obtained for an Ising fluid therefore also apply to symmetrical mixtures and, accordingly, results for Ising mixtures to ternary mixtures.

Finally, another motivation for studying magnetic fluids is that they exhibit a rich variety of critical phenomena in the phase diagram, which are worth investigating in their own right. While the pure fluids show symmetric and unsymmetric tricritical points as well as critical end points, the mixture of a magnetic fluid features tricritical lines, lines of critical end points, and lines of magnetic critical points.

A large number of papers dealing with magnetic fluids has been published so far, using mean-field theory [15–20], density functional theory [21–23], integral equation methods [14,24–28], the hierarchical reference theory [29], or Monte Carlo simulations [14,21,23,24,30–33]. Mostly, the liquid-vapor phase transition in the absence of a magnetic field was investigated, but some studies also focused on the magnetic order-disorder transition [29,30,32,34,35] or the influence of an external field [14,20,25,27,28,36]. However, most of these works treated ideal Ising or Heisenberg fluids, and all were restricted to pure magnetic fluids. A study of mixtures of ideal or nonideal magnetic fluids and a nonmagnetic fluid was missing so far, until we published in [37] the mean-field theory for mixtures of an Ising fluid and a van der Waals fluid. The subsequent goal was to perform Monte Carlo simulations and compare the obtained phase diagrams with the mean-field ones, in order to find out whether the topologies predicted by the theory would also show up in the presence of fluctuations. Since the mean-field approximation is a rather crude one, one could not expect quantitative coincidence with the simulations, and therefore the phase diagrams were only qualitatively compared. Also, it was no aim to determine exact locations of (tri)critical points or values of critical exponents, but rather to get an idea of the overall phase behavior in the three-dimensional thermodynamic phase diagram.

To explore as much of the phase diagrams as possible, several Monte Carlo (MC) techniques in various ensembles were adapted to the systems under consideration, ranging from the standard Gibbs ensemble method [38] to techniques that have not been applied to continuous-space fluids until only several years ago, like the histogram reweighting scheme [39,40].

We will now give a brief outline of this paper. In the following section, the mean-field theory of Ising mixtures will be reviewed, showing new phase diagrams of typical examples for each occurring topology, including the case of the ideal Ising mixture that was not covered in [37]. Section III will focus on the simulation methods we have used, especially the multihistogram reweighting technique applied to the semigrand and the isobaric-isothermal ensemble. In Sec. IV, the simulations performed for the Ising mixtures will be described and the results will be presented in the form of T,x and p,x as well as three-dimensional T,p,x diagrams. A short conclusion and summary of the results will finally round off the work.

II. MEAN-FIELD THEORY

A. General model

Consider a binary mixture in the molar volume v consisting of a van der Waals fluid (fluid 1) and an Ising fluid (fluid 2). The mole fraction of the second component shall be denoted as x and its magnetization per particle as m. The system is described by a van der Waals one-fluid equation of state,

$$p(T,v,x,m) = \frac{RT}{v-b} - \frac{a(x,m)}{v^2}, \tag{1}$$

where R is the molar gas constant, the attraction parameter a is defined according to the quadratic mixing rule as

$$a(x,m) = a_{11}(1-x)^2 + 2a_{12}x(1-x) + \left(a_{22} + \frac{1}{2}a_m m^2\right)x^2, \tag{2}$$

and the size parameter b is assumed constant. In Eq. (2), a_{11} and a_{22} denote the nonmagnetic interactions between particles of the same kind, a_{12} the nonmagnetic interaction between unlike particles, and a_m the magnetic interaction in the Ising fluid. If $a_m=0$, the model becomes identical to the mean-field description of binary van der Waals mixtures by van Konynenburg and Scott [41]. For the magnetization, the equation of state in the absence of a magnetic field reads

$$m(T,v,x) = \tanh\left(\frac{a_m x m}{vRT}\right). \tag{3}$$

The molar Helmholtz free energy of the system corresponding to Eqs. (1) and (3) with respect to the reference state of an ideal unmixed gas with molar volume $v^0=b$ is given by

$$\begin{aligned} f^{rel}(T,v,x,m) &= f(T,v,x,m) - f^0(T,v^0) \\ &= x f_s(T,m) + RT[(1-x)\ln(1-x) + x\ln x] \\ &\quad - RT\ln\left(\frac{v-b}{b}\right) - \frac{a(x,m)}{v}, \end{aligned} \tag{4}$$

where

$$f_s(T,m) = RT\left(\frac{1-m}{2}\ln\frac{1-m}{2} + \frac{1+m}{2}\ln\frac{1+m}{2}\right) \tag{5}$$

is the entropy part of the free energy of the Ising fluid component. The mixture can be characterized by the three reduced parameters ζ, Λ, and R_m,

$$\zeta = \frac{a_{22}-a_{11}}{a_{11}+a_{22}}, \quad \Lambda = \frac{a_{11}-2a_{12}+a_{22}}{a_{11}+a_{22}}, \quad R_m = \frac{1}{2}\frac{a_m}{a_{22}}. \tag{6}$$

Now one can define dimensionless variables scaled by the critical parameters of component 2,

$$T_r = \frac{27}{8}\frac{bRT}{a_{22}} = \frac{27}{4}R_m\frac{bRT}{a_m}, \quad p_r = \frac{27b^2p}{a_{22}}, \quad v_r = \frac{v}{b}. \tag{7}$$

The conditions for the coexistence of two phases α and β at a temperature T_0 and pressure p_0 are given by

$$p(x_\alpha,v_\alpha,m_\alpha) = p(x_\beta,v_\beta,m_\beta) = p_0, \tag{8}$$

$$\mu_1(x_\alpha,v_\alpha) = \mu_1(x_\beta,v_\beta), \tag{9}$$

$$\mu_2(x_\alpha,v_\alpha,m_\alpha) = \mu_2(x_\beta,v_\beta,m_\beta), \tag{10}$$

$$m_\alpha = m(x_\alpha,v_\alpha), \quad m_\beta = m(x_\beta,v_\beta). \tag{11}$$

By solving these equations numerically, one can find the first-order phase transition surfaces in x,T,p space.

Instead of a Curie line, the three-dimensional phase diagram of the mixture exhibits a surface of magnetic phase transitions or Curie surface as it can be called. It is defined as the set of points where the magnetization m as a solution of the magnetic equation of state (3) goes to zero, given by

$$v = \frac{xa_m}{RT}. \tag{12}$$

Inserting this into Eq. (1) and setting $m=0$ gives the equation of the Curie surface in x,T,p space.

Lines of second-order phase transitions (plait point and consolute point lines) are calculated from the equations

$$\left(\frac{\partial^2 g}{\partial x^2}\right)_{T,p} = 0, \quad \left(\frac{\partial^3 g}{\partial x^3}\right)_{T,p} = 0, \tag{13}$$

where $g=f-(\partial f/\partial v)v$ is the molar Gibbs free energy. Expressing these conditions in terms of the Helmholtz free energy yields

$$f_{2v}f_{2x} - f_{vx}^2 = 0, \tag{14}$$

$$f_{3v}f_{2x}^2 - 3f_{2vx}f_{vx}f_{2x} + 3f_{v2x}f_{vx}^2 - f_{3x}f_{2v}f_{vx} = 0, \tag{15}$$

$$f_{3x}f_{2v}^2 - 3f_{2xv}f_{vx}f_{2v} + 3f_{x2v}f_{vx}^2 - f_{3v}f_{2x}f_{vx} = 0, \quad (16)$$

where

$$f_{ivjx} \equiv \left(\frac{\partial^{i+j}f}{\partial v^i \partial x^j}\right)_T. \quad (17)$$

In the case of a tricritical line the first of these conditions taken in the limit of $m \to 0$ yields an analytic expression for the tricritical temperature as a function of the mole fraction x. It turns out that depending on the three mixture parameters, the tricritical line has either the character of a consolute point line and goes to infinite pressure (type-A behavior) or it resembles a plait point line and eventually becomes unstable in a tricritical end point (type-B). In the three-dimensional parameter space, the boundary surface separating these two types of behavior is described by the equation

$$\Lambda = -\frac{R_m}{4}(1+\zeta). \quad (18)$$

If

$$\Lambda + \frac{R_m}{4}(1+\zeta) > 0, \quad (19)$$

the system is of type A; otherwise, it is of type B.

B. Ideal Ising mixture

Equations (1)–(4) describe the general case of a mixture where both components have van der Waals interactions characterized by the parameters a_{11}, a_{12}, and a_{22} and particles belonging to the second species show an additional magnetic interaction of strength a_m. However, there are certain special cases of the system with not all interactions present which still show quite an interesting phase behavior. This section will focus on the simplest possible case featuring magnetic interaction, but no van der Waals interaction at all ($a_{11}=a_{12}=a_{22}=0$). It corresponds to the mixture of an ideal Ising fluid ($R_m=\infty$) and a hard-sphere fluid. Apart from excluding a fraction of the volume, the nonmagnetic species in this case does not interact at all, such that the system can be considered a diluted ideal Ising fluid. On the other hand, it can also be seen as the limiting case of an Ising mixture where the magnetic interparticle force is much stronger than any other interaction in the system.

The reduced free energy of an Ising mixture with $a_{ij}=0$ is given by

$$f_r \equiv \frac{bf}{a_m} = xT_r\left(\frac{1-m}{2}\ln\frac{1-m}{2} + \frac{1+m}{2}\ln\frac{1+m}{2}\right) - T_r\ln(v_r-1) - \frac{1}{2}\frac{x^2m^2}{v_r} + T_r[(1-x)\ln(1-x) + x\ln x]. \quad (20)$$

The reduced temperature T_r and pressure p_r are now defined as

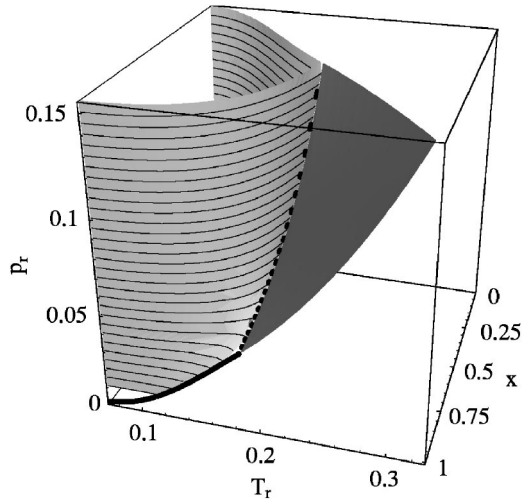

FIG. 1. x,T,p diagram of an ideal Ising mixture. Thick line, liquid-vapor curve of the pure Ising fluid; thin lines, isobaric curves on the first-order surface; dotted line, tricritical line; dark surface, Curie surface; light surface, coexistence surface of para-ferro first-order transitions.

$$T_r = \frac{bRT}{a_m}, \quad p_r = \frac{b^2p}{a_m}, \quad (21)$$

since the previous definitions (7) were based on the critical temperature and pressure of component 2, which are now zero. As one can see, there is no parameter left in the free energy (20). In order to find the first-order phase transitions, conditions (8)–(11) have to be applied, with the constraint that now one of the phases always has a finite magnetization m and the magnetization of the other phase is zero.

Having no van der Waals interactions, the system lacks a line of critical points. However, it exhibits a tricritical line starting at the tricritical point of the ideal Ising fluid and going to infinite pressure (type-A behavior), which complies with condition (19) if Λ and ζ are considered as indeterminate but finite quantities here. The equation of the tricritical line is rather simple for this mixture: namely,

$$T_t = x_t - \sqrt{x_t\left(x_t - \frac{1}{3}\right)}, \quad \frac{1}{3} \leqslant x_t \leqslant 1. \quad (22)$$

It lies on the surface of magnetic phase transitions which, according to Eq. (12), is given by

$$v_r = \frac{x}{T_r} \quad (23)$$

or, inserting into (1) with $m=0$,

$$p_r = \frac{T_r^2}{x - T_r}. \quad (24)$$

For $p_r \to \infty$, it reaches the limiting point $T_t^\infty = x_t^\infty = \frac{1}{3}$.

Figure 1 shows the three-dimensional phase diagram of the ideal Ising mixture and Fig. 2 sections at constant pressures and temperatures.

An interesting feature of this system is that in the limit of infinite pressure its mean-field description becomes equiva-

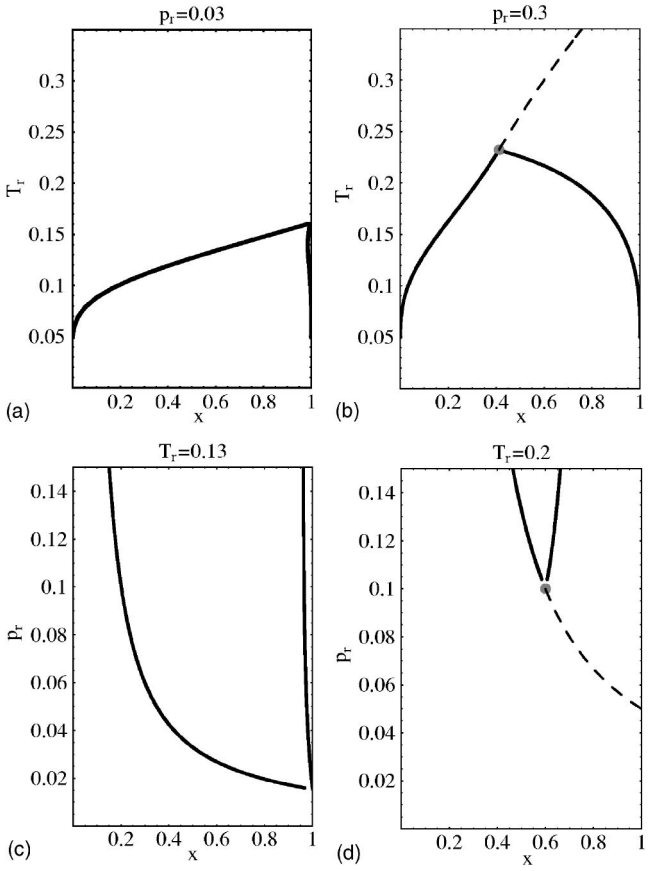

FIG. 2. Constant-p and -T sections of the phase diagram in Fig. 1. Thick line, para-ferro phase coexistence curve; dashed line, Curie line; gray dot, tricritical point.

lent to that of the well-known BEG model [8], or rather a special case of it, known as the Blume-Capel model [8,42,43] (see Appendix A for a detailed derivation). It can also be shown that the general version of the BEG model is obtained by applying the same limit to the mixture of an ideal Ising fluid and a van der Waals fluid.

C. Nonideal Ising mixtures

Consider now the case that both species also exhibit a nonmagnetic van der Waals interaction. Thus, the spin particles now interact with each other both via magnetic and nonmagnetic forces and they also interact with particles of the other component.

Contrary to the special case of the mixture with an ideal Ising fluid, in the general case the coexistence of two phases α and β with nonzero magnetizations m_α and m_β is also possible. The system exhibits a tricritical as well as a critical line. The latter one can in general show one of five different topologies, depending on the values of the parameters ζ and Λ. These are the types I–V described by van Konynenburg and Scott in [41]. For the sake of simplicity, only cases with a continuous critical line connecting the critical points of the two pure components are considered here, restricting the values of ζ and Λ to the region of type I in the global phase diagram. However, this only applies to nonmagnetic critical lines. The inclusion of the magnetic equation of state in Eqs. (14)–(16) leads to additional solutions with respect to those in [41]: namely, critical lines with a finite magnetization (see the Appendix of [37]). These lines occur especially at high pressures in the form of consolute point lines where demixing into two magnetic liquid phases sets in.

As to the tricritical line, it can appear in the two topologies described in Sec. II A. In the case of type A, the line approaches infinite pressure at a concentration

$$x_t^\infty = \frac{4\Lambda + R_m(1+\zeta)}{4\Lambda + 3R_m(1+\zeta)} \tag{25}$$

and temperature $T_t^\infty = (27R_m/4)x_t^\infty$.

As examples illustrating the occurring topologies one representative of each type, A and B, was chosen, whose complete three-dimensional phase diagrams are shown in Fig. 3, whereas in Figs. 4 and 5 sections through these diagrams at constant values of pressure or temperature are displayed.

For the type-A system, Fig. 3(a), R_m was chosen corresponding to an Ising fluid of type III in the nomenclature introduced in [33]. Accordingly, the pure magnetic component shows a critical, but no tricritical point. Still, a tricritical line shows up in the mixture which has the character of a pure demixing line, starting at infinite pressure in $x_t^\infty = 0.0526$, $T_t^\infty = 0.0533$ and ending in a tricritical end point on the gas-liquid coexistence surface. Below the tricritical temperature, the system demixes into a ferromagnetic, 2-rich liquid and a paramagnetic, 1-rich liquid. An examination of the

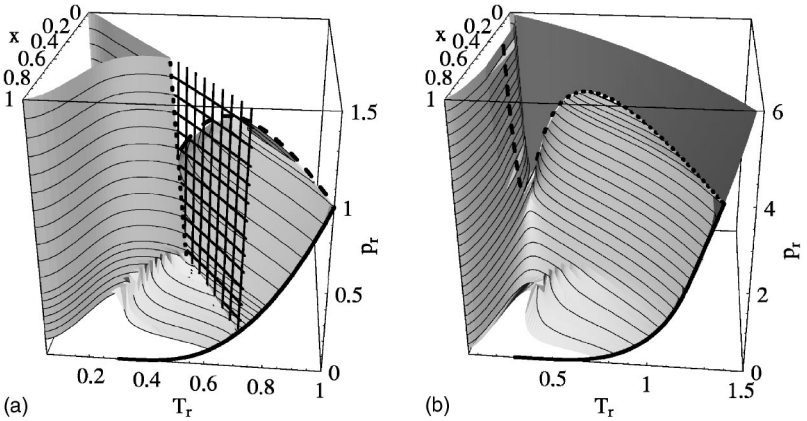

FIG. 3. x,T,p diagrams of Ising mixtures with (a) $\zeta=0.5$, $\Lambda=-0.05$, $R_m=0.15$ and (b) $\zeta=0.5$, $\Lambda=-0.25$, $R_m=0.4$. System (a) is of type A, whereas system (b) is of type B. Thick line, liquid-vapor curve of the pure Ising fluid component; thin lines, isobaric curves on the first-order surface; dotted line, tricritical line; dashed line, critical line; hatched surface in (a) and dark surface in (b), surface of magnetic phase transitions; light surface, surface of first-order phase transitions.

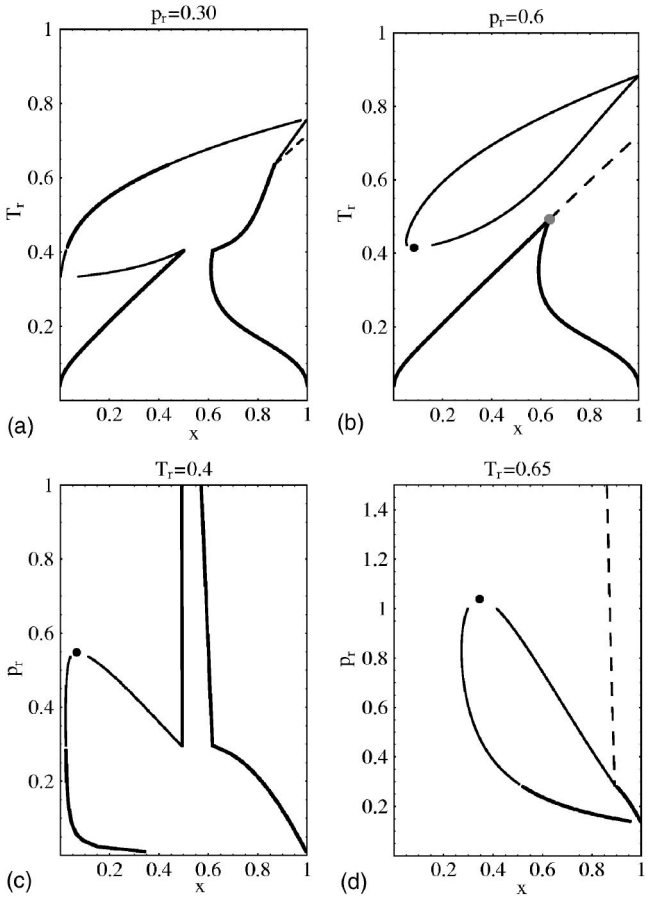

FIG. 4. Constant-p and -T sections of the phase diagram in Fig. 3(a). Thick line, para-ferro phase coexistence curve; thin line, para-para phase coexistence curve; dashed line, Curie line; gray dot, tricritical point; black dot, critical point.

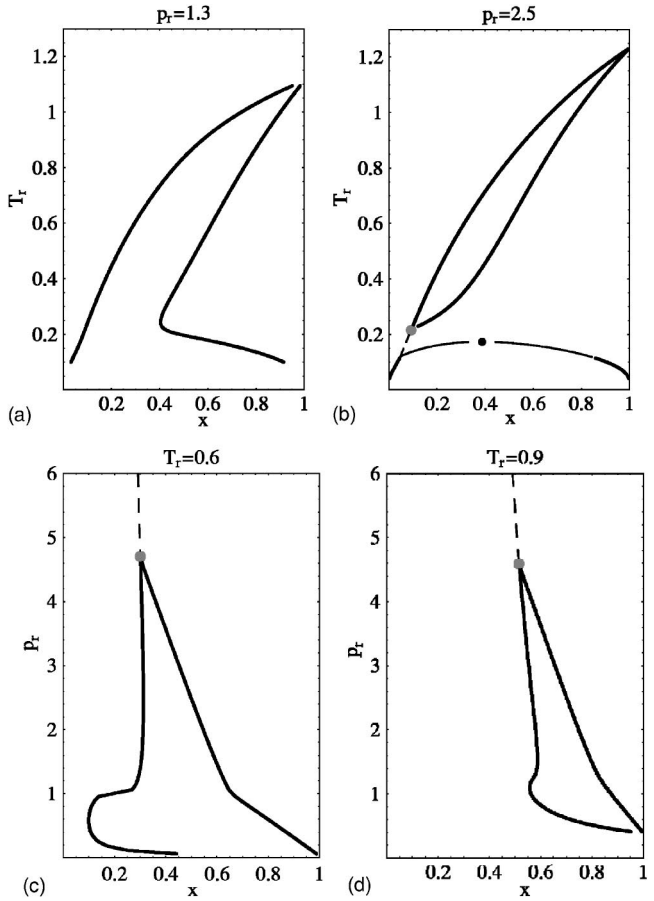

FIG. 5. Constant-p and -T sections of the phase diagram in Fig. 3(b). Thick line, para-ferro phase coexistence curve; thin line, ferro-ferro phase coexistence curve; dashed line, Curie line; gray dot, tricritical point; black dot, magnetic critical point.

phase behavior for $p \to \infty$ reveals that the tricritical line becomes metastable at high pressures and instead a line of magnetic consolute points appears, accompanied with a demixing transition into two ferromagnetic liquid phases, which persists up to infinite pressure. The Curie surface seen in Fig. 3(a) is bounded by the Curie line of the pure Ising fluid at $x=1$, the tricritical line, and a line of critical end points that connects the critical end point of the Ising fluid and the tricritical end point.

In the type-B case shown in Fig. 3(b), R_m was chosen to be in the type-I region of the Ising fluid parameter space, and thus there is only a tricritical point present in the pure magnetic component. From there, the tricritical line emerges, but contrary to the type-A topology, it reaches a maximum pressure value and then drops down again, ending in a tricritical end point. It has the character of a plait point line, below which a phase transition from paramagnetic gas to ferromagnetic liquid occurs. However, similar to the type-A mixtures at high pressure, the system also exhibits a demixing transition, where the mixture resolves into two ferromagnetic liquid phases with different concentrations and magnetizations. These phases become identical in a magnetic critical point. A line of such points starts in a magnetic critical end point on the first-order coexistence surface and continues up to infinite pressure. The Curie surface is now bounded by the Ising fluid Curie line, the tricritical line, and a line of critical end points along which it intersects the first-order demixing surface. Since the type-I Ising fluid has no stable critical point, the critical line extending from the plait point of the van der Waals fluid also becomes metastable when it hits the surface of first-order para-ferro phase transitions [this is not visible in Fig. 3(b)].

III. SIMULATION DETAILS

Besides simulations in the well-known Gibbs ensemble [38,44] we have also carried out calculations within the semigrand ensemble [45]. In combination with the histogram reweighting technique [39,40], it provides better efficiency especially near the critical regions, and it avoids the disadvantage of particle insertion and deletion moves that restrict the accessible density and temperature range for the simulations considerably. Since the application of histogram reweighting to the semigrand ensemble needs some consideration, we will explain this point in detail.

In the case of a grand-canonical simulation, one can compile a two-dimensional histogram of the observed total potential energy and particle number, $H(U,N)$ at a certain system inverse temperature $\beta=1/k_BT$ and chemical potential μ.

Then the (normalized) histogram will provide an estimate of the grand-canonical probability distribution $P_{\beta\mu}(U,N)$ according to

$$H_{\beta\mu}(U,N) \approx P_{\beta\mu}(U,N) = \frac{\Omega(U,N)e^{-\beta U+\beta\mu N}}{\Xi(\beta,\mu)}, \quad (26)$$

where $\Omega(U,N)$ is the microcanonical and $\Xi(\beta,\mu)$ the grand-canonical partition function, given by

$$\Xi(\beta,\mu) = \sum_U \sum_N \Omega(U,N)e^{-\beta U+\beta\mu N}. \quad (27)$$

Using Eq. (26), one can obtain an estimate for the distribution function $P_{\beta'\mu'}(U,N)$ by "reweighting" $H_{\beta\mu}(U,N)$:

$$P_{\beta'\mu'}(U,N) \approx \frac{\Xi(\beta,\mu)}{\Xi(\beta',\mu')}e^{-(\beta'-\beta)U+(\beta'\mu'-\beta\mu)N}H_{\beta\mu}(U,N)$$
$$\propto e^{-U\delta\beta+N\delta\mu_r}H_{\beta\mu}(U,N), \quad (28)$$

where $\delta\beta \equiv \beta'-\beta$, $\mu_r \equiv \beta\mu$, and $\delta\mu_r \equiv \mu_r'-\mu_r$.

The idea behind the multihistogram method is now to perform a number of n simulations at different parameters β_i,μ_i whose histograms cover the whole region of interest in the U,N plane. Provided there is enough overlap between neighboring histograms, it is then possible to interpolate histograms at intermediate thermodynamic states β,μ that were not simulated beforehand. If the simulations have a length of K_i observations, the n histograms $H_i(U,N)$ can be combined into an estimated distribution function $P_{\beta\mu}(U,N)$ in the following way [40]:

$$P_{\beta\mu}(U,N) = \frac{\sum_{i=1}^{n} H_i(U,N)e^{-\beta U+\beta\mu N}}{\sum_{i=1}^{n} K_i e^{-\beta_i U+\beta_i\mu_i N-C_i}}. \quad (29)$$

The reweighting factors C_i occurring in Eq. (29) have to be calculated self-consistently via the condition

$$e^{C_i} = \sum_N \sum_U P_{\beta_i\mu_i}(U,N), \quad (30)$$

for example, by doing a simple iteration.

Now contrary to pure fluids, the phase behavior of a binary mixture is fully covered only in a three-dimensional phase diagram—for example, in concentration-temperature-pressure space. Accordingly, reweighting to another state point in general requires to specify a three-dimensional difference vector to the new state point. If one looks at the probability distribution in the semigrand ensemble, which can be written as

$$P_{\beta p\Delta}(U,V,N_2) = \frac{\Omega(U,V,N_2)e^{-\beta U-\beta pV+\beta\Delta N_2}}{Y(\beta,p,\Delta)}, \quad (31)$$

where $\Delta=\mu_2-\mu_1$, $\Omega(U,V,N_2)$ is the density of states, and $Y(\beta,p,\Delta)$ the semigrand-canonical partition function, given by

$$Y(\beta,p,\Delta) = \sum_U \sum_V \sum_{N_2} \Omega(U,V,N_2)e^{-\beta U-\beta pV+\beta\Delta N_2}, \quad (32)$$

it can be seen that the reweighting scheme for Eq. (31) yields

$$P_{\beta'p'\Delta'}(U,V,N_2)$$
$$\propto e^{-(\beta'-\beta)U-(\beta'p'-\beta p)V+(\beta'\Delta'-\beta\Delta)N_2}H_{\beta p\Delta}(U,V,N_2)$$
$$= e^{-U\delta\beta-V\delta p_r+N_2\delta\Delta_r}H_{\beta p\Delta}(U,V,N_2), \quad (33)$$

with $\delta p_r \equiv p_r'-p_r$, $p_r \equiv \beta p$, $\delta\Delta_r \equiv \Delta_r'-\Delta_r$, and $\Delta_r \equiv \beta\Delta$. Thus, instead of just replacing the factor $e^{-U\delta\beta+N\delta\mu_r}$ occurring in Eq. (28) with $e^{-U\delta\beta+N_2\delta\Delta_r}$, one needs an additional factor $e^{-V\delta p_r}$ and, more importantly, one has to store a three-dimensional histogram $H(U,V,N_2)$. It turns out, however, that in the special cases when either $\delta\beta$ or $\delta p \equiv p'-p$ is chosen as zero, it is again sufficient to use a two-dimensional histogram.

Most evidently, reweighting at constant temperature ($\delta\beta=0$) eliminates the total energy U from Eq. (33), yielding

$$P_{\beta p'\Delta'}(V,N_2) \propto e^{-V\delta p_r+N_2\delta\Delta_r}H_{\beta p\Delta}(V,N_2), \quad (34)$$

such that only the histogram $H(V,N_2)$ needs to be recorded during the simulation. The constant pressure case ($\delta p=0$) is a bit more subtle, however, since $\delta p=0$ does not imply $\delta p_r=0$. Instead, one obtains

$$P_{\beta'p\Delta'}(U,V,N_2) \propto e^{-U\delta\beta-V(\beta'p-\beta p)+N_2\delta\Delta_r}H_{\beta p\Delta}(U,V,N_2)$$
$$= e^{-(U+pV)\delta\beta+N_2\delta\Delta_r}H_{\beta p\Delta}(U,V,N_2), \quad (35)$$

which indicates that the proper quantity to be stored is in this case the enthalpy $E=U+pV$. Hence, one can write

$$P_{\beta'p\Delta'}(E,N_2) \propto e^{-E\delta\beta+N_2\delta\Delta_r}H_{\beta p\Delta}(E,N_2), \quad (36)$$

for the reweighting procedure at constant pressure. Comparing Eqs. (34) and (36) with Eq. (28) shows that the reweighting scheme for a binary mixture in the semigrand ensemble at constant temperature or pressure takes the same form as that of a pure fluid in a grand-canonical ensemble, making its application not more computationally extensive. One can even use the same program to reweight the binary mixture and the pure fluid histograms.

Following the same arguments as in the pure fluid case, one can also perform multiple-histogram reweighting in the semigrand ensemble. If all n simulations were done at the same temperature β but at different pressures p_i and chemical potential differences Δ_i, the formulas

$$P_{\beta p\Delta}(V,N_2) = \frac{\sum_{i=1}^{n} H_i(V,N_2)e^{-\beta pV+\beta\Delta N_2}}{\sum_{i=1}^{n} K_i e^{-\beta p_i V+\beta\Delta_i N_2-C_i}} \quad (37)$$

and

$$e^{C_i} = \sum_V \sum_{N_2} P_{\beta p_i\Delta_i}(V,N_2) \quad (38)$$

apply, whereas for combining n histograms obtained at the same pressure p but different temperatures β_i and chemical potential differences Δ_i, one has to use

$$P_{\beta p\Delta}(E,N_2)=\frac{\sum_{i=1}^{n}H_i(E,N_2)e^{-\beta E+\beta\Delta N_2}}{\sum_{i=1}^{n}K_i e^{-\beta_i E+\beta_i\Delta_i N_2-C_i}} \tag{39}$$

and

$$e^{C_i}=\sum_E\sum_{N_2}P_{\beta_i p\Delta_i}(E,N_2). \tag{40}$$

Finding the coexistence curve at constant p or β is now analogous to the pure fluid case. One calculates the one-dimensional concentration distribution $P_{\beta p\Delta}(N_2)=\Sigma_V P_{\beta p\Delta}(V,N_2)$ or $P_{\beta p\Delta}(N_2)=\Sigma_E P_{\beta p\Delta}(E,N_2)$. By tuning Δ and applying the equal-area criterion for the peaks in the distribution of the mole fraction $x=N_2/N$, the equilibrium concentrations are found, and thus a T, x or p, x phase diagram can be built up.

If one is interested in the distribution of the magnetization rather than the concentration, as is the case if one wants to determine the locus of second-order magnetic phase transitions in an Ising mixture, a similar procedure can be applied. The partition function of a magnetic fluid simulated in the isobaric-isothermal ensemble at constant temperature, pressure, and magnetic field H is given by

$$Z(\beta,p,H)=\sum_U\sum_V\sum_M\Omega(U,V,M)e^{-\beta U-\beta pV+\beta HM}, \tag{41}$$

with M being the total magnetization and $\Omega(U,V,M)$ the density of states, and the corresponding probability distribution by

$$P_{\beta pH}(U,V,M)=\frac{\Omega(U,V,M)e^{-\beta U-\beta pV+\beta HM}}{Z(\beta,p,H)}. \tag{42}$$

Since the phase transition one is interested in occurs only at $H=0$, the term including the magnetization vanishes. As in the semigrand ensemble, it is again convenient to perform the reweighting method either at constant pressure or constant temperature. In the first case one has

$$P_{\beta' p}(E,M)\propto e^{-E\delta\beta}H_{\beta p}(E,M) \tag{43}$$

or

$$P_{\beta p}(E,M)\propto\frac{\sum_{i=1}^{n}H_i(E,M)e^{-\beta E}}{\sum_{i=1}^{n}K_i e^{-\beta_i E-C_i}} \tag{44}$$

and

$$e^{C_i}=\sum_E\sum_M P_{\beta_i p}(E,M). \tag{45}$$

On the other hand, if $\beta'=\beta$, one can write

$$P_{\beta p'}(V,M)\propto e^{-V\delta p_r}H_{\beta p}(V,M) \tag{46}$$

and, for multiple histograms,

$$P_{\beta p}(V,M)\propto\frac{\sum_{i=1}^{n}H_i(V,M)e^{-\beta pV}}{\sum_{i=1}^{n}K_i e^{-\beta p_i V-C_i}}, \tag{47}$$

with

$$e^{C_i}=\sum_V\sum_M P_{\beta p_i}(V,M). \tag{48}$$

IV. MC SIMULATIONS

A. Ideal Ising mixture

As a model for the interaction in an ideal Ising mixture—i.e., a mixture of an ideal Ising fluid and a hard-sphere fluid—the potential $u_{ij}(r)$ was chosen as

$$u_{ij}(r)=\begin{cases}u_{sc}(r)+s_i s_j J(r), & r<r_c,\\ 0, & r>r_c,\end{cases} \tag{49}$$

with $J(r)$ being a Yukawa potential,

$$J(r)=-\varepsilon\frac{e^{-(r-\sigma)/\sigma}}{r/\sigma}, \tag{50}$$

and $u_{sc}(r)$ having the form of a Lennard-Jones potential truncated at the minimum and shifted up by the well depth to give a repulsive potential smoothly decaying to zero:

$$u_{sc}(r)=\begin{cases}4\epsilon\left[\left(\frac{\sigma}{r}\right)^{12}-\left(\frac{\sigma}{r}\right)^{6}\right]+\epsilon, & r<\sqrt[6]{2}\sigma,\\ 0, & r\geqslant\sqrt[6]{2}\sigma.\end{cases} \tag{51}$$

Such a soft-core potential is often referred to as a Weeks-Chandler-Andersen (WCA) potential. The spins s_i are defined in such a way that they are either +1 or −1 if the particle is of species 2 (the ideal Ising fluid) and zero if it is of species 1 (the hard-sphere fluid). Thus, only the magnetic particles feel an attractive interaction between each other, whereas the nonmagnetic ones just repell each other at short distances.

The size of the particles is assumed equal for both species and denoted by σ, and $r=|\mathbf{r}_i-\mathbf{r}_j|$ is the interparticle distance. Periodic boundary conditions were applied, and the potential $u_{ij}(r)$ was truncated at a cutoff distance r_c equal to half the length of the simulation box. This truncation was accounted for by adding an appropriate long-range correction. The strength ϵ of the WCA potential was set equal to the strength ε of the Yukawa potential.

To locate the phase equilibria and construct the three-dimensional phase diagram of the ideal Ising mixture, the following simulation methods were applied: the constant-pressure Gibbs ensemble, the semigrand ensemble combined with multihistogram reweighting, and the isobaric-isothermal ensemble together with the cumulant intersection method to locate the surface of second-order magnetic phase transitions.

The Gibbs ensemble simulations were performed with a total number of particles N of 500 or 1000 for runs close to the critical region. They were arranged in cycles consisting of N trial particle displacements, N_2 spin-flip attempts, one volume change attempt, and a number of particle swap attempts which was chosen to yield about 1%–3% of the particles being swapped in one cycle. Typically, the number of performed cycles was about 10^6. In all the Gibbs ensemble simulations, the excluded volume map sampling (EVMS)

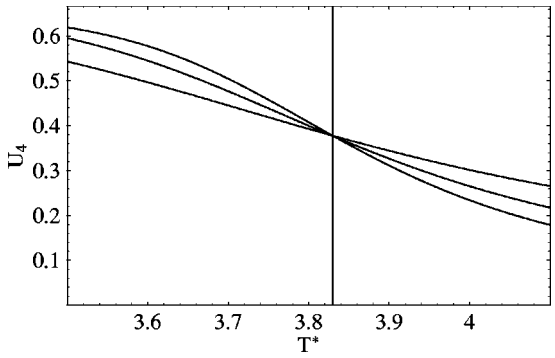

FIG. 6. The fourth-order cumulant ratio U_4 as a function of temperature and system size ($N=150$, 300, and 500) for the ideal Ising mixture at a concentration of $x=0.4$ and a pressure of $p^*=3$. The lines result from multihistogram reweighting. The critical temperature $T_c^*=3.83$ obtained from the intersection point is indicated as a vertical line.

method [46] was utilized in order to facilitate runs at higher densities.

The simulations in the semigrand ensemble were conducted with a particle number of $N=300$. Typical runs consisted of 4×10^9 MC steps, where one step was either an attempted identity change, a trial particle displacement, a spin-flip attempt, or a volume rearrangement attempt. Depending on whether reweighting at constant pressure or at constant temperature was to be performed, either the observed values of the volume or those of the enthalpy were stored together with the number of particles of species 2 in a histogram with 300 bins in both dimensions. From the combined histograms of all simulations at a certain pressure or temperature, the coexistence concentrations in the phase diagram were then obtained via multi-histogram reweighting.

Points on the Curie surface were found via the cumulant intersection technique [47,48]. Simulations in the constant-NpT ensemble were carried out, consisting of about 10^9 Monte Carlo steps, each of which was either a trial particle displacement, a trial spin-flip or a volume rearrangement attempt. During these runs, two-dimensional V, M or E, M histograms, respectively, were obtained and afterwards extrapolated to other temperatures or pressures via the multihistogram reweighting technique. Thus, the fourth-order cumulant ratio U_4 of the magnetization distribution $P(m)$, defined as

$$U_4 = 1 - \frac{\langle m^4 \rangle}{3\langle m^2 \rangle^2} \tag{52}$$

with the kth moment of m given by

$$\langle m^k \rangle = \int m^k P(m) dm, \tag{53}$$

could be calculated as a function of T or p. This was done for three different system sizes $N=150$, $N=300$, and $N=500$, and the intersection point of the resulting curves was determined as an estimate for the critical temperature or pressure of the infinite system. Figure 6 shows a typical plot for $x=0.4$ and $p^*=3$. For the interaction potential (49) with long-range correction we find a critical cumulant ratio of $U_{4c} \approx 0.38$, just as in the pure Ising fluid case with $x=1$ (using a truncated potential as in [29] for the pure fluid, we reproduce their value of $U_{4c} \approx 0.46$). In the case of the mixture a weak concentration dependence of U_{4c} was observed, similar to the density dependence in the pure fluid.

The results of the simulations are presented in Figs. 7 and 8. Figure 7(a) shows T, x phase diagrams obtained at several constant pressures, including Curie lines, and Fig. 7(b) p, x coexistence curves and Curie lines calculated at constant temperature. These curves at constant p or T are cross sections of the complete three-dimensional phase diagram of the studied system and can be qualitatively compared with the corresponding sections calculated in mean-field theory (Fig. 2). As one can see, the phase behavior is quite similar, with demixing into a paramagnetic and a ferromagnetic phase. Since the critical regions were not investigated thoroughly within this study, the question whether the ideal Ising mixture exhibits a line of tricritical points as predicted by

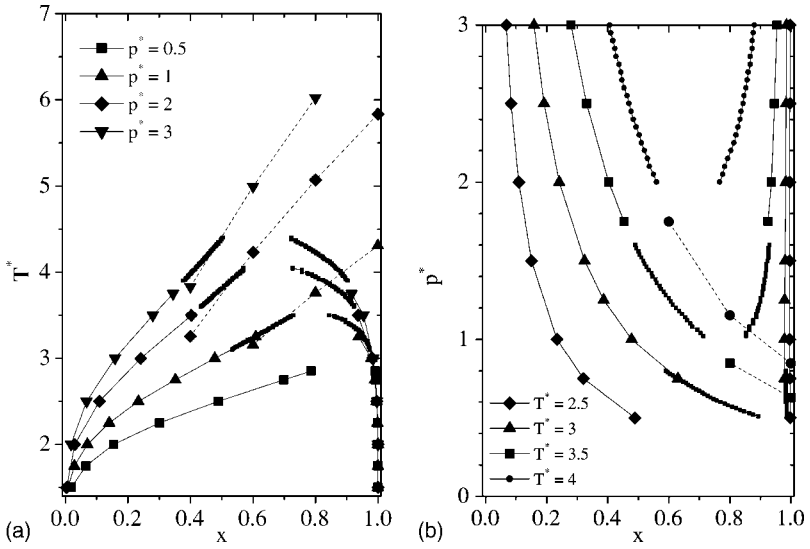

FIG. 7. (a) T, x phase diagrams of the ideal Ising mixture at different pressures ($p^*=0.5$, 1, 2, and 3) from MC calculations. (b) p, x phase diagrams of the ideal Ising mixture at different temperatures ($T^*=2.5$, 3, 3.5, and 4) obtained from MC calculations. Large symbols, Gibbs ensemble simulations; small symbols, semigrand ensemble simulations and multihistogram reweighting; symbols connected with dashed lines, para-ferro magnetic critical points at fixed concentrations obtained from the cumulant intersection method. All lines are only guides to the eye.

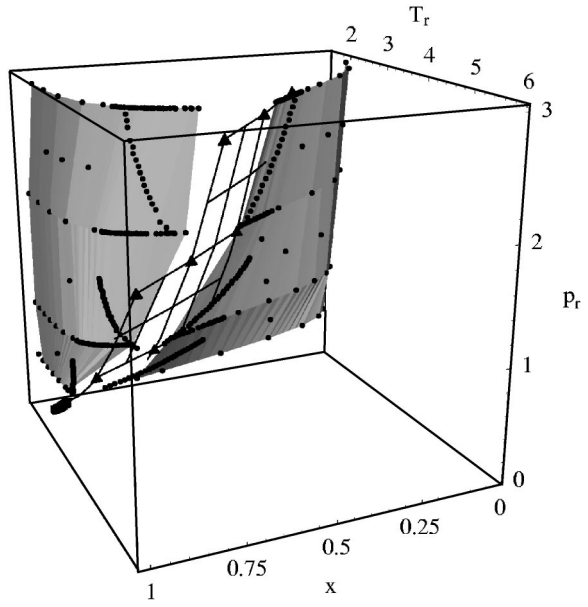

FIG. 8. *x*, *T*, *p* phase diagram of the ideal Ising mixture obtained from MC calculations. Circles, data from Gibbs ensemble and semigrand ensemble simulations; triangles, para-ferro magnetic critical points obtained with the cumulant intersection method. All lines and surfaces are only guides to the eye.

mean-field theory remains unanswered. However, as far as the simulations go, they do not rule out the existence of such a tricritical line.

An even better impression of the overall topology of the whole phase diagram is given in Fig. 8, where the isothermal and isobaric cross sections are assembled into a three-dimensional *x*, *T*, *p* diagram. Comparison with Fig. 1 shows the agreement with the mean-field topology.

B. Nonideal Ising mixtures

For the general mixture of an Ising and a van der Waals fluid, the interaction potential used is

$$u_{ij}(r) = \begin{cases} u_{LJ}(r) + s_i s_j J(r), & r < r_c, \\ 0, & r > r_c, \end{cases} \tag{54}$$

where the spin-dependent interaction part only enters if both particles belong to the magnetic component ($s_i = 0$ for particles of species 1, the van der Waals fluid, and $s_i = \pm 1$ otherwise). Also, the Lennard-Jones interaction strength ε now depends on the species *a* and *b* of the two particles,

$$u_{LJ}(r) = 4\varepsilon_{ab}\left[\left(\frac{\sigma}{r}\right)^{12} - \left(\frac{\sigma}{r}\right)^{6}\right], \tag{55}$$

and the Yukawa potential is accordingly given by

$$J(r) = -R\varepsilon_{22}\frac{e^{-(r-\sigma)/\sigma}}{r/\sigma}, \tag{56}$$

such that *R* corresponds to the ratio of magnetic and nonmagnetic interaction strengths of the Ising fluid component. One can then define parameters ζ and Λ in analogy to Eq. (6) with ε_{11}, ε_{12}, and ε_{22} instead of a_{11}, a_{12}, and a_{22}.

Again, all simulations were performed with periodic boundary conditions, the cutoff radius r_c was half the box length, and tail correction terms were added to the potential energy to compensate for the truncation of the potential.

Phase diagrams of the nonideal Ising mixture were investigated with Gibbs ensemble simulations at constant pressure in the case of first-order phase transitions, as well as simulations in the constant-*NpT* ensemble and the cumulant crossing technique for the second-order para-ferro phase transitions. Moreover, the first-order transitions were also investigated with the semigrand ensemble and multihistogram reweighting.

The simulations in the Gibbs ensemble were performed with a total number of particles *N* of 500 or 1000 for runs near the critical region. They were arranged in cycles consisting of *N* trial particle displacements, N_2 spin-flip attempts, one volume change attempt, and a number of particle interchange attempts chosen to yield about 1%–3% of the particles being swapped in one cycle. Typically, about 10^6 cycles were performed per simulation run. The EVMS method was applied in order to facilitate runs at higher densities.

Simulations in the semigrand ensemble were conducted with a particle number of $N = 300$ and a typical length of 4×10^9 MC steps, where one step was either an attempted identity change, a trial particle displacement, a spin-flip attempt, or a volume rearrangement attempt. Depending on whether reweighting at constant pressure or at constant temperature was to be performed, either the observed values of the volume or those of the enthalpy were stored together with the number of particles of species 2 in a histogram with 300 bins in both dimensions. From the combined histogram of all simulations at a certain pressure or temperature, the coexistence concentrations of the phase diagram were then obtained via multihistogram reweighting.

Points on the Curie surface were found via the cumulant intersection technique. During simulations in the constant-*NpT* ensemble, consisting of about 10^9 MC steps, the two-dimensional *E*, *M* histograms were obtained and extrapolated to other temperatures via the multihistogram reweighting technique. Thus, the fourth-order cumulant ratio of the magnetization distribution $P(m)$ could be calculated as a function of temperature. This was done for three different system sizes $N = 150$, $N = 300$, and $N = 500$, and the intersection point of the resulting curves was determined as an estimate for the critical temperature of the infinite system.

In order to find out whether the two phase diagram topologies found in mean-field theory are also observed in Monte Carlo simulations, two systems were studied, whose parameter values correspond to the examples given in Sec. II C—namely, $\zeta = 0.5$, $\Lambda = -0.05$, $R = 0.05$ for a type-A mixture and $\zeta = 0.5$, $\Lambda = -0.25$, $R = 0.1333$ for a type-B mixture. The values of *R* were chosen as representatives of type-I and -III Ising fluids according to the results of the simulations of the pure nonideal Ising fluid [33].

1. Type A

Figures 9 and 10 show *T*,*x* diagrams of the type-A mixture at $p^* = p\sigma^3/\varepsilon_{22} = 0.08$ and $p^* = 0.15$ and *p*,*x* diagrams at

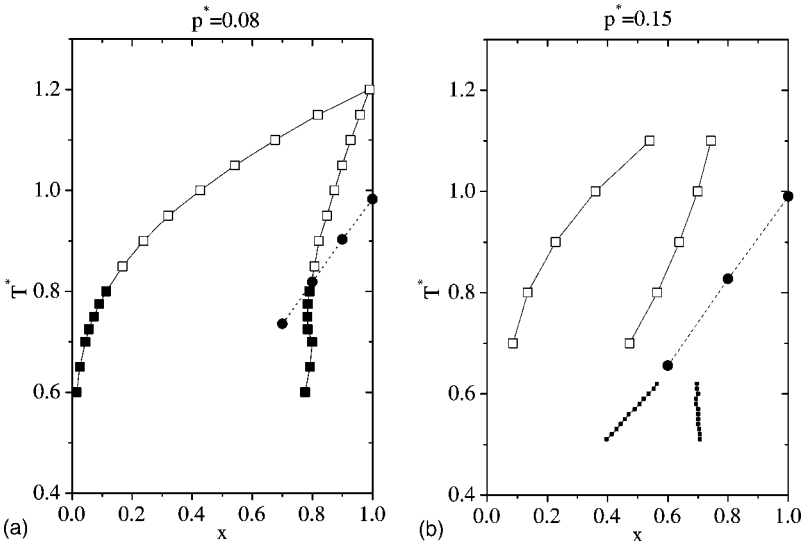

FIG. 9. T,x phase diagrams of the Ising mixture with $\zeta=0.5$, $\Lambda=-0.05$, and $R=0.05$ at different pressures ($p^*=0.08$ and 0.15) obtained from MC calculations. Large squares, Gibbs ensemble simulations; small squares, semigrand ensemble simulations and multihistogram reweighting; circles, para-ferro magnetic critical points at certain concentrations obtained with the cumulant intersection method. Solid symbols indicate para-ferro phase coexistence, open symbols para-para coexistence. All lines are only guides to the eye.

$T^*=k_BT/\varepsilon_{22}=0.6$ and $T^*=0.9$. At $p^*=0.08$, the system exhibits a critical end point where the Curie line intersects the phase coexistence curve, separating first-order para-para phase transitions occurring at temperatures above from para-ferro phase transitions below the critical end point temperature. A similar phase behavior is seen in mean-field theory [Fig. 4(a)]. The features predicted for low temperatures at this pressure were not found in the simulations, however, due to the limitation of the accessible temperature range, resulting from low acceptance probabilities in the particle interchange steps. At a higher pressure value, $p^*=0.15$, the Curie line does not connect to the para-para gas-liquid two-phase region, which has now become a separate area. Instead, it obviously passes into a para-ferro first-order demixing transition via a tricritical point, just as in the mean-field picture [Fig. 4(b)]. This behavior also shows nicely in the constant-T diagram in Fig. 10(a). Clearly, a triple point can be observed, above which para-para gas-liquid and para-ferro liquid-liquid transitions coexist separately, whereas below only a transition from paramagnetic gas to ferromagnetic liquid is present, which is exactly the topology predicted by mean-field theory [Fig. 4(c)]. At a higher temperature [$T^*=0.9$, Fig. 10(b)], the liquid-liquid transition has vanished and, instead, there is a para-para and a para-ferro gas-liquid transition, separated by a critical end point, the same way as in the mean-field calculations [Fig. 4(d)].

To get an idea of the topology of the whole phase diagram in x,T,p space, the two-dimensional x,T and x,p diagrams shown in Figs. 9 and 10, together with some additional ones, are assembled in a three-dimensional plot (Fig. 11). The extrapolated loci of the tricritical demixing points are also included, connected by a line as an estimate for the tricritical line. Comparison with the type-A mean-field diagram [Fig. 3(a)] leads to the conclusion that the mean-field topology is also found in the Monte Carlo simulations, at least in the accessible temperature range.

2. Type B

T,x and p,x sections of the type-B Ising mixture phase diagram can be seen in Figs. 12 and 13. Both constant-pressure diagrams, obtained at $p^*=0.175$ and $p^*=0.24$, show para-ferro gas-liquid phase transitions in the whole temperature range, and all calculated points of the Curie surface lie inside the two-phase region. This is in agreement with the

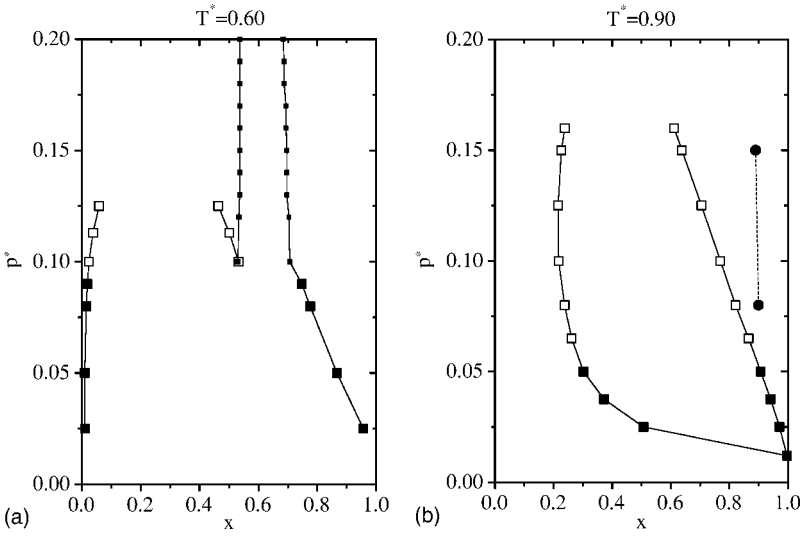

FIG. 10. p,x phase diagrams of the Ising mixture with $\zeta=0.5$, $\Lambda=-0.05$, and $R=0.05$ at different temperatures ($T^*=0.6$ and 0.9) obtained from MC calculations. Large squares, Gibbs ensemble simulations; small squares, semigrand ensemble simulations and multihistogram reweighting; circles, para-ferro magnetic critical points obtained via linear interpolation of the Curie lines at $p^*=0.08$ and 0.15 (Fig. 9) to $T^*=0.9$. Solid symbols indicate para-ferro phase coexistence, open symbols para-para coexistence. All lines are only guides to the eye.

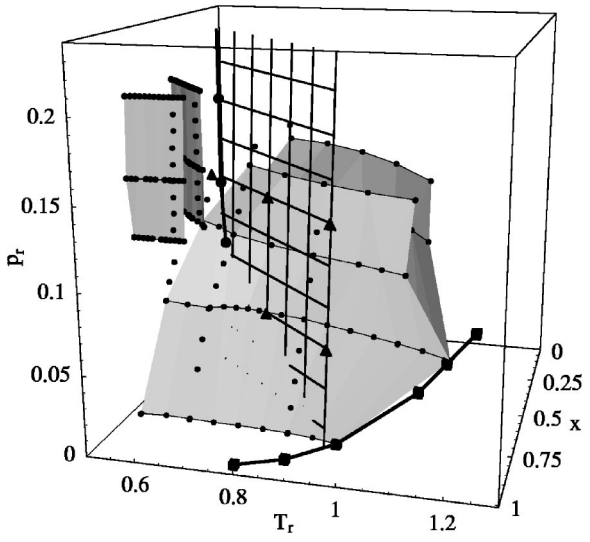

FIG. 11. x,T,p phase diagram of the Ising mixture with $\zeta=0.5$, $\Lambda=-0.05$, and $R=0.05$ from MC calculations. Small circles, data from Gibbs ensemble and semigrand ensemble simulations Large circles, tricritical points obtained via linear extrapolation of the demixing binodals; triangles, para-ferro magnetic critical points obtained with the cumulant intersection method. The squares correspond to the liquid-vapor curve of the pure Ising fluid. All lines and surfaces are only guides to the eye.

mean field diagrams in Figs. 5(a) and 5(b). The features occurring at low temperatures in the mean-field diagram with $p_r=2.5$—namely, the tricritical point and the demixing transition into two ferromagnetic phases—could not be found by the simulations, however. The reason was not so much the failure of the Monte Carlo methods due to the small acceptance probabilities at such low temperatures, but the occurrence of a liquid-solid transition before these temperatures are reached. Since the applied mean-field theory does not allow for solid phases *a priori*, this transition does not show up in the corresponding mean-field phase diagrams.

The p,x diagrams displayed in Fig. 13 show very nice compliance with mean-field theory. Both isothermal sections, obtained at $T^*=0.8$ and $T^*=1.2$, exhibit para-ferro gas-liquid transitions in the whole pressure range. While the gas branch of the binodal is curved at lower temperatures, a crossover can be observed when going to higher temperatures, where both branches show a pronounced linear shape, quite the same as in the mean-field diagrams in Figs. 5(c) and 5(d), strongly suggesting tricritical behavior. The positions of the supposed tricritical points were determined by linear extrapolation of the liquid and gas branches of the binodals and are indicated in Fig. 13.

All isobaric and isothermal sections were subsequently compiled to build up the three-dimensional x,T,p phase diagram of the type-B Ising mixture, shown in Fig. 14. The line connecting the extrapolated tricritical points can be seen to hit a pressure maximum and then bend down again at lower temperature, the same way the tricritical line does in the mean-field diagram [Fig. 3(b)]. Thus one can say that it has the character of a gas-liquid plait point line, and therefore the mean-field topology is also present in the regions of the phase diagram that were covered by the Monte Carlo calculations. The magnetic critical line showing up at low temperatures in the mean-field diagram, however, does not appear in the Monte Carlo diagram, as it is oppressed by the presence of the solid phase in the simulated system.

V. CONCLUSION

In this paper we have presented the results of Monte Carlo simulations investigating first- and second-order phase transitions in mixtures of an Ising fluid and a nonmagnetic fluid. Since for Ising mixtures there are at the moment only phase diagrams available which were obtained within mean-field theory, the investigations of these systems were restricted to a topological comparison with the phase diagrams from Monte Carlo calculations. Nevertheless, it turned out that the mean-field theory provides quite a good prediction of the qualitative phase behavior. The two types of tricritical lines that occur in the mean-field diagrams, one having plait point character and one behaving like a consolute point line, could both be verified in the computer simulations. Of course, the

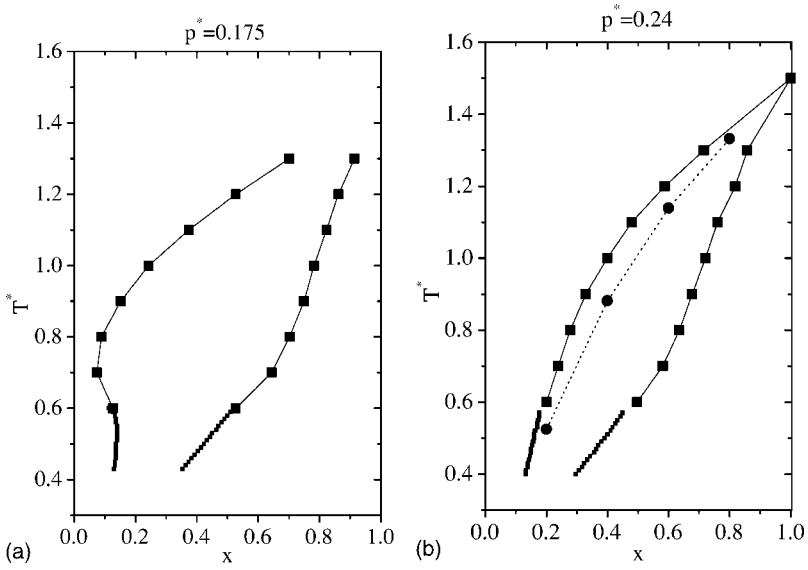

FIG. 12. T,x phase diagrams of the Ising mixture with $\zeta=0.5$, $\Lambda=-0.25$, and $R=0.1333$ at different pressures ($p^*=0.175$ and 0.24) obtained from MC calculations. Large squares, Gibbs ensemble simulations; small squares, semigrand ensemble simulations and multihistogram reweighting; circles, para-ferro magnetic critical points at certain concentrations obtained with the cumulant intersection method. Solid symbols indicate para-ferro phase coexistence. All lines are only guides to the eye.

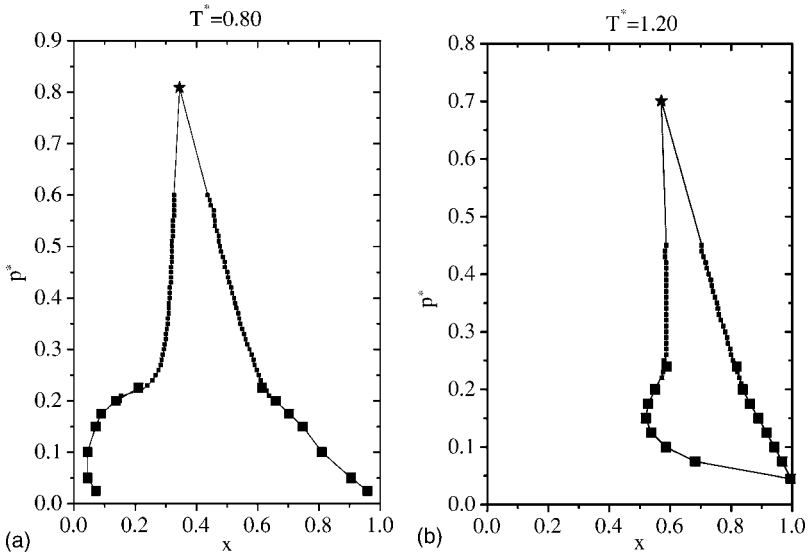

FIG. 13. p,x phase diagrams of the Ising mixture with $\zeta=0.5$, $\Lambda=-0.25$, and $R=0.1333$, at different temperatures ($T^*=0.8$ and 1.2) obtained from MC calculations. Large squares, Gibbs ensemble simulations; small squares, semigrand ensemble simulations and multihistogram reweighting; stars, tricritical points obtained from linear extrapolation of the binodals. Solid symbols indicate para-ferro phase coexistence. All lines are only guides to the eye.

MC calculations were restricted to a limited temperature range and therefore could not probe the whole thermodynamic space covered by the mean-field diagrams. Furthermore, it was found that the existence of a solid phase cannot be ignored because it prohibits the formation of certain features predicted by the mean-field theory, such as the demixing transition into two magnetic liquid phases at very low temperatures. Therefore, the inclusion of solid phases into the mean-field description of the Ising mixture (using, e.g., the theory in [49]) would be a possible improvement. Another task to be undertaken in the future is the application of an integral equation theory such as the soft mean spherical approximation (SMSA) used in [14] to mixtures of an Ising and a Lennard-Jones fluid, thus allowing a quantitative comparison with the phase diagrams obtained in the computer simulations. First, however, the theory has to be adapted to the nonideal Ising fluid itself, using a Yukawa potential for the magnetic and a Lennard-Jones potential for the nonmagnetic interaction. Both these undertakings are planned for the near future.

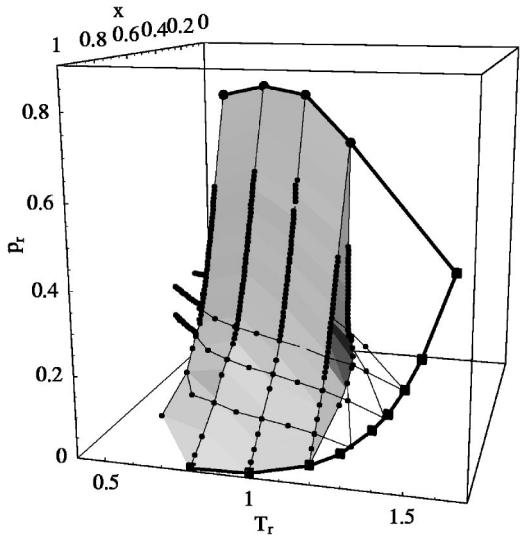

FIG. 14. x,T,p phase diagram of the Ising mixture with $\zeta=0.5$, $\Lambda=-0.25$, and $R=0.1333$ from MC calculations. Small circles, data from Gibbs ensemble and semigrand ensemble simulations; large circles, tricritical points obtained via linear extrapolation of the binodals. The squares correspond to the liquid-vapor curve of the pure Ising fluid. All lines and surfaces are only guides to the eye.

ACKNOWLEDGMENT

We acknowledge support by the Fonds zur Förderung der wissenschaftlichen Forschung under Project No. P15247-TPH.

APPENDIX: IDEAL ISING MIXTURE IN THE LIMIT $p \to \infty$

From Eq. (20) one can derive the pressure, the relative activities λ_1^* and λ_2^* and the magnetization of the ideal Ising mixture as

$$p_r = \frac{T_r}{v_r - 1} - \frac{1}{2}\frac{x^2 m^2}{v_r^2}, \tag{A1}$$

$$\ln \lambda_1^* \equiv \frac{\mu_1 - \mu_1^0}{RT} = \ln \frac{1-x}{v_r - 1} + \frac{v_r}{v_r - 1}, \tag{A2}$$

$$\ln \lambda_2^* \equiv \frac{\mu_2 - \mu_2^0}{RT} = -\frac{xm^2}{v_r T_r} + \frac{1-m}{2} \ln \frac{1-m}{2} + \frac{1+m}{2} \ln \frac{1+m}{2} + \ln \frac{x}{v_r - 1} + \frac{v_r}{v_r - 1}, \tag{A3}$$

$$m = \tanh\left(\frac{xm}{v_r T_r}\right). \tag{A4}$$

Now Eq. (A3) can be simplified using Eq. (A4), since

$$\frac{1-m}{2}\ln\frac{1-m}{2}+\frac{1+m}{2}\ln\frac{1+m}{2}$$
$$=\frac{1}{2}\left(\ln\frac{1-m}{2}+\ln\frac{1+m}{2}\right)+\frac{m}{2}\ln\frac{1+m}{1-m}$$
$$=\frac{1}{2}\ln\frac{1-m^2}{4}+m\tanh^{-1}m$$
$$=\ln\frac{\sqrt{1-m^2}}{2}+\frac{xm^2}{v_rT_r}. \tag{A5}$$

Then, Eq. (A3) becomes

$$\ln\lambda_2^*=\ln\frac{\sqrt{1-m^2}}{2}+\ln\frac{x}{v_r-1}+\frac{v_r}{v_r-1}. \tag{A6}$$

Using Eqs. (A1), (A2), and (A6), the conditions for phase equilibrium, Eqs. (8)–(10), become

$$\frac{T_r}{v_\alpha-1}-\frac{1}{2}\frac{x_\alpha^2m^2}{v_\alpha^2}=p_0, \tag{A7}$$

$$\frac{T_r}{v_\beta-1}=p_0, \tag{A8}$$

$$\ln\frac{1-x_\alpha}{v_\alpha-1}+\frac{v_\alpha}{v_\alpha-1}=\ln\frac{1-x_\beta}{v_\beta-1}+\frac{v_\beta}{v_\beta-1}, \tag{A9}$$

$$\ln\sqrt{1-m^2}+\ln\frac{x_\alpha}{v_\alpha-1}+\frac{v_\alpha}{v_\alpha-1}=\ln\frac{x_\beta}{v_\beta-1}+\frac{v_\beta}{v_\beta-1}. \tag{A10}$$

These equations have to be solved in combination with the magnetic equation of state for phase α,

$$m=\tanh\left(\frac{x_\alpha m}{v_\alpha T_r}\right). \tag{A11}$$

According to Eq. (A1), taking the limit $p_r\to\infty$ corresponds to $v_r\to1$. Since Eqs. (A7)–(A10) have diverging terms when applying this limit directly, one has to be more careful. The pressure p_0 itself can be eliminated by equating Eqs. (A7) and (A8),

$$\frac{T_r}{v_\alpha-1}-\frac{1}{2}\frac{x_\alpha^2m^2}{v_\alpha^2}=\frac{T_r}{v_\beta-1}. \tag{A12}$$

We will now switch to the variables α and β instead of v_α and v_β, defined via $v_\alpha\equiv1+\alpha$ and $v_\beta\equiv1+\beta$, and apply the limits $\alpha\to0$ and $\beta\to0$ in the end. Equation (A12) then becomes

$$-\frac{1}{2}\frac{x_\alpha^2m^2}{T_r(1+\alpha)^2}=\frac{\alpha-\beta}{\alpha\beta}. \tag{A13}$$

Similarly, Eq. (A9) can be written as

$$\ln\frac{1-x_\alpha}{1-x_\beta}=\ln\frac{\alpha}{\beta}+\frac{\alpha-\beta}{\alpha\beta}, \tag{A14}$$

which can be combined with Eq. (A13) to give

$$\ln\frac{1-x_\alpha}{1-x_\beta}+\frac{1}{2}\frac{x_\alpha^2m^2}{T_r(1+\alpha)^2}=\ln\frac{\alpha}{\beta}. \tag{A15}$$

Finally, Eq. (A10) yields

$$\ln\frac{x_\alpha}{x_\beta}+\ln\sqrt{1-m^2}=\ln\frac{\alpha}{\beta}+\frac{\alpha-\beta}{\alpha\beta} \tag{A16}$$

or, with Eq. (A13),

$$\ln\frac{x_\alpha}{x_\beta}+\frac{1}{2}\frac{x_\alpha^2m^2}{T_r(1+\alpha)^2}+\ln\sqrt{1-m^2}=\ln\frac{\alpha}{\beta}. \tag{A17}$$

In Eqs. (A15) and (A17) one can now take the limit $\alpha,\beta\to0$, where

$$\lim_{\alpha,\beta\to0^+}\ln\frac{\alpha}{\beta}=\ln1=0.$$

Together with the magnetic equation of state (A11) with $v_\alpha=1$, one then obtains

$$\ln\frac{1-x_\alpha}{1-x_\beta}+\frac{1}{2}\frac{x_\alpha^2m^2}{T_r}=0, \tag{A18}$$

$$\ln\frac{x_\alpha}{x_\beta}+\frac{1}{2}\frac{x_\alpha^2m^2}{T_r}+\ln\sqrt{1-m^2}=0, \tag{A19}$$

$$m=\tanh\left(\frac{x_\alpha m}{T_r}\right), \tag{A20}$$

as conditions for a first-order phase equilibrium at $p_r=\infty$. These are only three equations instead of five, as in Eqs. (A7)–(A11), but since both $v_\alpha=1$ and $v_\beta=1$, there are only the three variables x_α, x_β, and m left to determine.

As was already pointed out in Sec. II B, at $p_r=\infty$ a tricritical point is present at $T_t^\infty=x_t^\infty=\frac{1}{3}$. With Eq. (23), the Curie line at $p_r=\infty$ is given by

$$T_r=x. \tag{A21}$$

Consider now the Blume-Capel (BC) model. Its Hamiltonian is given by

$$H=-J\sum_{\langle i,j\rangle}S_iS_j+\Delta\sum_iS_i^2, \tag{A22}$$

where Δ is the crystal field and J the coupling constant. Each lattice site is associated with a spin variable S_i that can take the values 0 and ±1. A ^{3}He atom at site i corresponds to $S_i=0$ and a ^{4}He atom to $S_i=\pm1$. As order parameters one has a "magnetization" M,

$$M=\langle S_i\rangle, \tag{A23}$$

corresponding to the superfluid ordering, and the concentration x of ^{4}He atoms,

$$x=\langle S_i^2\rangle. \tag{A24}$$

The mean-field equations for M and x read

$$x=\frac{2\cosh\beta\mathcal{J}M}{e^{\beta\Delta}+2\cosh\beta\mathcal{J}M}, \tag{A25}$$

$$M = \frac{2\sinh \beta\mathcal{J}M}{e^{\beta\Delta} + 2\cosh \beta\mathcal{J}M}, \tag{A26}$$

where $\beta = 1/k_B T$ is now the inverse temperature and $\mathcal{J} = zJ$ with z being the number of nearest neighbors. As the mean-field expression for the free energy per particle one obtains

$$\frac{F}{N} = \frac{1}{2}\mathcal{J}M^2 - \frac{1}{\beta}\ln[2e^{-\beta\Delta}\cosh \beta\mathcal{J}M + 1]. \tag{A27}$$

Regarding phase coexistence, there is always one phase with $M=0$ and one phase with $M \neq 0$. If $M \neq 0$, one can divide Eq. (A26) by Eq. (A25) and get

$$M = x_\alpha \tanh \beta\mathcal{J}M, \tag{A28}$$

where x_α is the concentration of the magnetic phase, which is found from

$$x_\alpha = \frac{2\cosh \beta\mathcal{J}M}{e^{\beta\Delta} + 2\cosh \beta\mathcal{J}M}. \tag{A29}$$

The value of x_β corresponding to the nonmagnetic phase is according to Eq. (A25) given by

$$x_\beta = \frac{2}{e^{\beta\Delta} + 2}. \tag{A30}$$

Now two phases characterized by (x_α, M) and $(x_\beta, 0)$ are in equilibrium if they have the same free energy, yielding an additional condition for phase coexistence,

$$\frac{1}{2}\beta\mathcal{J}M^2 - \ln[2e^{-\beta\Delta}\cosh \beta\mathcal{J}M + 1] = -\ln[2e^{-\beta\Delta} + 1] \tag{A31}$$

or

$$\frac{1}{2}\beta\mathcal{J}M^2 = \ln\frac{e^{\beta\Delta} + 2\cosh \beta\mathcal{J}M}{e^{\beta\Delta} + 2}. \tag{A32}$$

Using Eqs. (A29) and (A30), this becomes

$$\frac{1}{2}\beta\mathcal{J}M^2 = \ln\frac{x_\beta}{x_\alpha} + \ln\cosh \beta\mathcal{J}M. \tag{A33}$$

Eliminating Δ from Eqs. (A29) and (A30) gives

$$\frac{x_\alpha(1-x_\beta)}{x_\beta(1-x_\alpha)} = \cosh \beta\mathcal{J}M \tag{A34}$$

or, with Eq. (A33),

$$\ln\frac{1-x_\alpha}{1-x_\beta} + \frac{1}{2}\beta\mathcal{J}M^2 = 0. \tag{A35}$$

Equations (A28), (A33), and (A35) together constitute the conditions for the coexistence of two phases at a temperature β. With

$$\frac{1}{\sqrt{1-m^2}} = \frac{1}{\sqrt{1-\tanh^2\left(\frac{x_\alpha m}{T_r}\right)}} = \cosh\left(\frac{x_\alpha m}{T_r}\right), \tag{A36}$$

Eqs. (A18)–(A20) are identical to Eqs. (A35), (A33), and (A28), since m is defined as

$$m = \frac{1}{N_2}\sum_{i=1}^{N} S_i, \tag{A37}$$

with N_2 being the number of particles with spin, and therefore

$$xm = \frac{N_2}{N}\frac{1}{N_2}\sum_{i=1}^{N} S_i = M. \tag{A38}$$

The reduced temperature in the BC model corresponding to T_r is obviously $T_r^{BEG} = 1/\beta\mathcal{J}$. Thus, the coexistence curves of the mean-field phase diagram are the same for the BC model and the ideal Ising mixture at $p=\infty$. Consequently, the locus of the tricritical point, $T_t^\infty = x_t^\infty = 1/3$, and the line of second-order phase transitions, $T_r = x$, are also identical [8].

[1] T. Albrecht, C. Bührer, M. Fähnle, K. Maier, D. Platzek, and J. Reske, Appl. Phys. A: Mater. Sci. Process. **65**, 215 (1997).
[2] J. Reske, D. M. Herlach, F. Keuser, K. Maier, and D. Platzek, Phys. Rev. Lett. **75**, 737 (1995).
[3] W. H. Stockmayer, J. Chem. Phys. **9**, 398 (1941).
[4] B. Groh and S. Dietrich, Phys. Rev. E **50**, 3814 (1994).
[5] B. Groh and S. Dietrich, Phys. Rev. Lett. **72**, 2422 (1994).
[6] K. S. Pitzer, Chem. Phys. Lett. **105**, 484 (1984).
[7] K. S. Pitzer, J. Phys. Chem. **99**, 13070 (1995).
[8] M. Blume, V. J. Emery, and R. B. Griffiths, Phys. Rev. A **4**, 1071 (1971).
[9] J. L. Cardy and D. J. Scalapino, Phys. Rev. B **19**, 1428 (1979).
[10] A. N. Berker and D. R. Nelson, Phys. Rev. B **19**, 2488 (1979).
[11] A. Maciołek, M. Krech, and S. Dietrich, Phys. Rev. E **69**, 036117 (2004).
[12] G. M. Schneider, Adv. Chem. Phys. **17**, 1 (1970).
[13] N. B. Wilding, F. Schmid, and P. Nielaba, Phys. Rev. E **58**, 2201 (1998).
[14] I. Omelyan, I. Mryglod, R. Folk, and W. Fenz, Phys. Rev. E **69**, 061506 (2004).
[15] P. C. Hemmer and D. Imbro, Phys. Rev. A **16**, 380 (1977).
[16] N. E. Frankel and C. J. Thompson, J. Phys. C **8**, 3194 (1975).
[17] A. Oukouiss and M. Baus, Phys. Rev. E **55**, 7242 (1997).
[18] J. M. Tavares, P. I. C. Teixeira, and M. M. Telo da Gama, Phys. Rev. E **58**, 3175 (1998).
[19] F. Schinagl, R. Folk, and H. Iro, Condens. Matter Phys. **2**, 313 (1999).
[20] W. Fenz, R. Folk, I. Mryglod, and I. Omelyan, Phys. Rev. E **68**, 061510 (2003).
[21] E. Lomba, J.-J. Weis, and C. F. Tejero, Phys. Rev. E **58**, 3426 (1998).
[22] J. M. Tavares, M. M. Telo da Gama, P. I. C. Teixeira, J.-J.

Weis, and M. J. P. Nijmeijer, Phys. Rev. E **52**, 1915 (1995).
[23] J.-J. Weis, M. J. P. Nijmeijer, J. M. Tavares, and M. M. Telo da Gama, Phys. Rev. E **55**, 436 (1997).
[24] E. Lomba, J.-J. Weis, N. G. Almarza, F. Bresme, and G. Stell, Phys. Rev. E **49**, 5169 (1994).
[25] T. G. Sokolovska and R. O. Sokolovskii, Phys. Rev. E **59**, R3819 (1999).
[26] T. G. Sokolovska, Physica A **253**, 459 (1998).
[27] F. Lado and E. Lomba, Phys. Rev. Lett. **80**, 3535 (1998).
[28] F. Lado, E. Lomba, and J. J. Weis, Phys. Rev. E **58**, 3478 (1998).
[29] M. J. P. Nijmeijer, A. Parola, and L. Reatto, Phys. Rev. E **57**, 465 (1998).
[30] M. J. P. Nijmeijer and J. J. Weis, Phys. Rev. E **53**, 591 (1996).
[31] N. B. Wilding and P. Nielaba, Phys. Rev. E **53**, 926 (1996).
[32] I. M. Mryglod, I. P. Omelyan, and R. Folk, Phys. Rev. Lett. **86**, 3156 (2001).
[33] W. Fenz and R. Folk, Condens. Matter Phys. **6**, 675 (2003).
[34] W. Korneta, Phys. Rev. E **64**, 041109 (2001).
[35] A. L. Ferreira and W. Korneta, Phys. Rev. E **57**, 3107 (1998).
[36] F. Schinagl, H. Iro, and R. Folk, Eur. Phys. J. B **8**, 113 (1999).
[37] W. Fenz and R. Folk, Phys. Rev. E **67**, 021507 (2003).
[38] A. Z. Panagiotopoulos, Mol. Phys. **61**, 813 (1987).
[39] A. M. Ferrenberg and R. H. Swendsen, Phys. Rev. Lett. **61**, 2635 (1988).
[40] A. M. Ferrenberg and R. H. Swendsen, Phys. Rev. Lett. **63**, 1195 (1989).
[41] P. H. van Konynenburg and R. L. Scott, Philos. Trans. R. Soc. London, Ser. A **298**, 495 (1980).
[42] M. Blume, Phys. Rev. **141**, 517 (1966).
[43] H. W. Capel, Physica (Amsterdam) **32**, 966 (1966).
[44] A. Z. Panagiotopoulos, N. Quirke, M. Stapleton, and D. J. Tildesley, Mol. Phys. **63**, 527 (1988).
[45] D. A. Kofke and E. D. Glandt, Mol. Phys. **64**, 1105 (1988).
[46] M. R. Stapleton and A. Z. Panagiotopoulos, J. Chem. Phys. **92**, 1285 (1990).
[47] K. Binder, Z. Phys. B: Condens. Matter **43**, 119 (1981).
[48] K. Binder, Phys. Rev. Lett. **47**, 693 (1981).
[49] A. Daanoun, C. F. Tejero, and M. Baus, Phys. Rev. E **50**, 2913 (1994).